Biochemical and Biophysical Research Communications 439 (2013) 419–426

Contents lists available at ScienceDirect

Biochemical and Biophysical Research Communications

journal homepage: www.elsevier.com/locate/ybbrc

The moyamoya disease susceptibility variant RNF213 R4810K (rs112735431) induces genomic instability by mitotic abnormality

Toshiaki Hitomi [a,1], Toshiyuki Habu [b,1], Hatasu Kobayashi [a], Hiroko Okuda [a], Kouji H. Harada [a], Kenji Osafune [c], Daisuke Taura [d], Masakatsu Sone [d], Isao Asaka [c], Tomonaga Ameku [c], Akira Watanabe [c], Tomoko Kasahara [c], Tomomi Sudo [c], Fumihiko Shiota [c], Hirokuni Hashikata [e], Yasushi Takagi [e], Daisuke Morito [f], Susumu Miyamoto [e], Kazuwa Nakao [d], Akio Koizumi [a,*]

[a] Department of Health and Environmental Sciences, Graduate School of Medicine, Kyoto University, Kyoto, Japan
[b] Radiation Biology Center, Kyoto University, Kyoto, Japan
[c] Center for iPS Cell Research and Application (CiRA), Kyoto University, Kyoto, Japan
[d] Department of Medicine and Clinical Science, Graduate School of Medicine, Kyoto University, Kyoto, Japan
[e] Department of Neurosurgery, Graduate School of Medicine, Kyoto University, Kyoto, Japan
[f] Faculty of Life Sciences, Kyoto Sangyo University, Kyoto, Japan

ARTICLE INFO

Article history:
Received 16 August 2013
Available online 27 August 2013

Keywords:
Moyamoya disease
iPS cells
Mitotic phase
Genomic instability
Rs112735431
MAD2

ABSTRACT

Moyamoya disease (MMD) is a cerebrovascular disease characterized by occlusive lesions in the Circle of Willis. The RNF213 R4810K polymorphism increases susceptibility to MMD. In the present study, we characterized phenotypes caused by overexpression of RNF213 wild type and R4810K variant in the cell cycle to investigate the mechanism of proliferation inhibition. Overexpression of RNF213 R4810K in HeLa cells inhibited cell proliferation and extended the time of mitosis 4-fold. Ablation of spindle checkpoint by depletion of mitotic arrest deficiency 2 (MAD2) did not shorten the time of mitosis. Mitotic morphology in HeLa cells revealed that MAD2 colocalized with RNF213 R4810K. Immunoprecipitation revealed an RNF213/MAD2 complex: R4810K formed a complex with MAD2 more readily than RNF213 wild-type. Desynchronized localization of MAD2 was observed more frequently during mitosis in fibroblasts from patients ($n = 3$, 61.0 ± 8.2%) compared with wild-type subjects ($n = 6$, 13.1 ± 7.7%; $p < 0.01$). Aneuploidy was observed more frequently in fibroblasts ($p < 0.01$) and induced pluripotent stem cells (iPSCs) ($p < 0.03$) from patients than from wild-type subjects. Vascular endothelial cells differentiated from iPSCs (iPSECs) of patients and an unaffected carrier had a longer time from prometaphase to metaphase than those from controls ($p < 0.05$). iPSECs from the patients and unaffected carrier had significantly increased mitotic failure rates compared with controls ($p < 0.05$). Thus, RNF213 R4810K induced mitotic abnormalities and increased risk of genomic instability.

1. Introduction

Moyamoya disease (MMD: MIM 607151) is characterized by occlusive lesions at the terminal portion of internal carotid arteries in the Circle of Willis [1,2]. It is now recognized as one of the major causes of stroke in adults and children worldwide [3–6]. RNF213 has been recognized as the susceptibility gene for MMD, and the p. R4810K polymorphism (rs112735431 or ss179362673: G > A; herein referred to as RNF213 R4810K) as a founder variant commonly found in East Asian (Japanese, Korean and Chinese) MMD patients [7].

We recently found that vascular endothelial cells developed from induced pluripotent stem cells (iPSECs) of patients with MMD, carrying RNF213 R4810K, had reduced angiogenic activity [8]. This was partially mediated by the down-regulation of *Securin* [8]. In addition to *Securin*, various mitosis-associated genes were down regulated in iPSECs from patients [8]. Furthermore, the overexpression of RNF213 R4810K inhibited the proliferation of human umbilical vein endothelial cells (HUVECs) [8]. The primary aim of our study was to characterize the phenotypes associated with RNF213 R4810K in the cell cycle.

* Corresponding author. Address: Department of Health and Environmental Sciences, Graduate School of Medicine, Kyoto University, Konoe-cho, Yoshida, Sakyo-ku, Kyoto 606-8501, Japan. Fax: +81 75 753 4458.
E-mail address: koizumi.akio.5v@kyoto-u.ac.jp (A. Koizumi).
[1] These authors contributed equally to this work.

0006-291X/$ - see front matter © 2013 Elsevier Inc. All rights reserved.
http://dx.doi.org/10.1016/j.bbrc.2013.08.067

2. Methods

2.1. Participants

We studied three probands from three unrelated families with MMD, a carrier of RNF213 R4810K and seven controls. Details of the patients were described previously [8] and in Table S1. We obtained written informed consent from all participants in this study. Our study was approved by the Institutional Ethical Review Board of Kyoto University.

2.2. Cell culture and transfection

Fibroblasts and HeLa cells were maintained in Dulbecco's Minimal Essential Medium (DMEM; Invitrogen, Tokyo, Japan) containing 10% fetal bovine serum (FBS; Japan Bioserum, Hiroshima, Japan). Fibroblasts from passages 3–5 were used for all experiments. Induced pluripotent stem cells (iPSCs) were maintained as previously reported [8,9].

An mCherry-tagged wild-type RNF213 or an mCherry-tagged RNF213 R4810 K was cloned into pcDNA3.1 (Invitrogen) (Fig. S1) [8]. To monitor the localization of MAD2, HeLa cells stably expressing EGFP-MAD2 were used. MAD2 cDNA cloned into pEGFP-C1 (Clontech Laboratories, Palo Alto, CA, USA) was introduced into HeLa cells, and a G418-resistant clone was verified by western blotting and fluorescent microscopy. The plasmid was introduced into HeLa cells using Lipofectamine 2000 (Invitrogen) and successfully transfected cells selected with 500 μg/ml G418 (Nacalai Tesque, Kyoto, Japan) for 10 days.

Transfection of small interfering RNAs (siRNAs) was conducted using Dharmafect (#1 or #3; Dharmacon, Lafayette, CO, USA) as previously reported [8]. We purchased and used RNF213 siRNA (Santa Cruz Biotechnology) and MAD2 siRNA (Santa Cruz Biotechnology) with control siRNA-A (Santa Cruz Biotechnology) used as controls.

2.3. Karyotyping

For karyotyping, fibroblasts from six controls (Control 1 to Control 6), one carrier, and three patients were treated with nocodazole (100 ng/ml) for 72 h. Well-isolated chromosomes were chosen and counted three times for each chromosome set. For each fibroblast culture, duplicate karyotyping experiments were conducted. For MAD2 staining, fibroblasts were treated with nocodazole (100 ng/ml) for 72 h, fixed with 4% paraformaldehyde and permeabilized in phosphate-buffered saline (PBS) containing 0.2% Triton X-100. An anti-MAD2 antibody (Covance, Berkeley, CA, USA) was used for immunostaining.

To evaluate chromosomal instability, six iPSC clones from controls (Control 1 to Control 7 except Control 4) and four from a carrier and patients were karyotyped (Table S1).

2.4. Colony formation assays

Following transfection, HeLa cells were reseeded at densities of 1×10^3 to 2.7×10^4 cells/100-mm dish and maintained in DMEM with 10% FBS for 5 days. Medium containing G418 (Nacalai Tesque) was exchanged twice a week. After 10 days, resistant colonies were scored using formalin fixation and crystal violet staining.

2.5. Time-lapse imaging using confocal laser scanning microscopy

Transfected HeLa cells and iPSECs were plated on 35-mm glass-bottom culture dishes. Time-lapse 3D imaging was performed using an FV10i confocal microscope (Olympus, Tokyo, Japan) at 37 °C/5% CO_2. The recording interval was 40 min, and Z-stack images were generated with Fluoview (Olympus).

2.6. Western blotting

Samples were subjected to immunoblotting using the anti-RNF213 antibody, which we generated previously [8], anti-MAD2, anti-dsRed (BD Biosciences), or anti-β-actin (Abcam, Cambridge, UK) antibodies. Quantitation was conducted using Image J software.

2.7. Co-immunoprecipitation of MAD2 with RNF213

HeLa cells transiently expressing the wild-type RNF213 mCherry or RNF213 R4810K mCherry or naïve HeLa cells were lysed in RIPA buffer without sodium dodecyl sulfate (SDS) but with protease inhibitors (Nacalai Tesque). Cell lysates from 4×10^6 cells were incubated with protein A agarose (Santa Cruz Biotechnology) for 30 min at 4 °C with normal mouse immunoglobulin G (IgG; MBL, Nagoya, Japan). After magnetic separation, beads were discarded and supernatants incubated for 4 h at 4 °C with a monoclonal anti-dsRed or polyclonal anti-RNF213 antibody [8] followed by magnetic beads for 4 h. Beads were washed three times with lysis buffer, and bound proteins dissolved in SDS sample buffer at 95 °C for 5 min, subjected to SDS polyacrylamide gel electrophoresis (PAGE) and analyzed by western blotting with anti-MAD2 antibody.

2.8. Statistical analysis

Results are presented as the mean ± standard deviation (SD) unless otherwise stated. Differences between groups were analyzed using analysis of variance (ANOVA), followed by Tukey's honestly significant difference test for comparisons involving more than two means (SAS Institute Inc., Cary, NC, USA). The variance in chromosome numbers as determined by karyotyping was compared with controls using an F-test. Subcellular localization of MAD2 was categorized into four groups and compared with controls using Fisher's exact test with Bonferroni correction. A p-value with Bonferroni correction less than 0.05 was considered statistically significant.

3. Results

3.1. Effects of RNF213 R4810K overexpression

mCherry-tagged wild-type RNF213 and/or RNF213 R4810K proteins (Fig. S1) were overexpressed in HeLa cells (Fig. S2A and B). Localization of exogenous RNF213 R4810K was similar to that of exogenous and endogenous wild-type RNF213, where proteins were observed in the cytoplasm around the nucleus (Fig. S2B). Overexpression of RNF213 R4810K highly repressed colony formation units of HeLa cells (Fig. S2C). In contrast, RNAi-mediated depletion of RNF213 in HeLa cells did not repress colony formation units (Fig. S2D).

To understand better the causes underlying inhibition of cell proliferation, cell cycle distribution of HeLa cells expressing wild-type RNF213 and RNF213 R4810K were monitored. Overexpression of RNF213 R4810K caused a G2/M-plus-higher-DNA-content (4N>) accumulation in HeLa cells (Fig. S3), but overexpression of wild-type of RNF213 did not. Live imaging analyses showed that mitotic stages were severely delayed in HeLa cells overexpressing RNF213 R4810K (Fig. 1A–C). In cells overexpressing the control vector, wild-type RNF213, control siRNA or RNF213 siRNA, the mean time from prometaphase to metaphase was 37 ± 10 min: The mean time

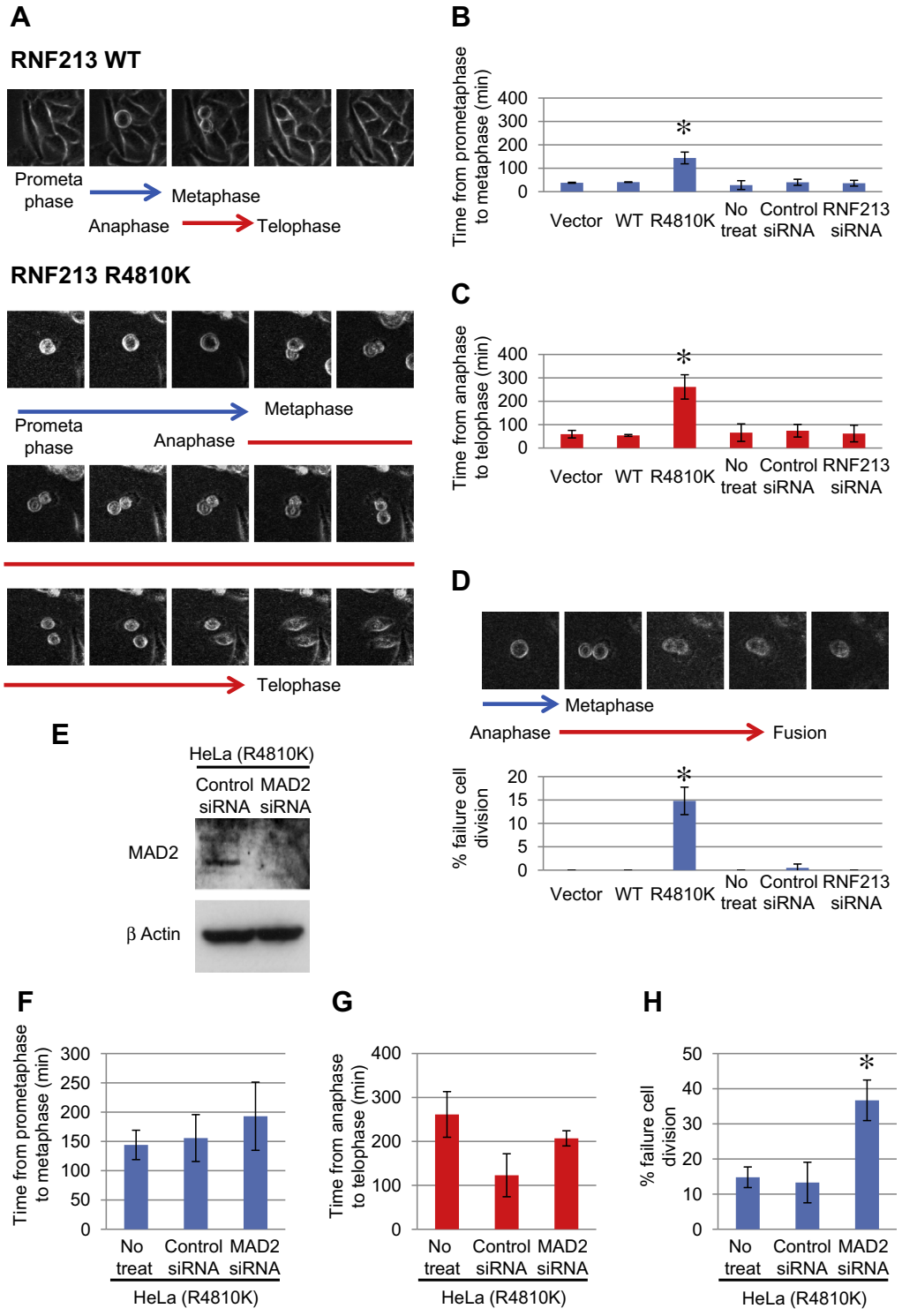

Fig. 1. Time-lapse imaging of HeLa cells transfected with wild-type RNF213 and RNF213 R4810K, or control siRNA, RNF213 siRNA and MAD2 siRNA. (A) Representative time-lapse images showing wild-type RNF213 and RNF213 R4810K. Images were obtained every 40 min. (E) Western blot analysis of HeLa cells overexpressing RNF213 R4810K with MAD2 siRNA transfection. (B, C, F, G) The period of time from prometaphase to metaphase, and from anaphase to telophase. A total of 20 cells were observed in three areas for each group. (D, H) Failed cell division in HeLa cells overexpressing RNF213 R4810K transfected with control siRNA and MAD2 siRNA. Cells ($n = 40$) were counted in three areas for each group. Values are presented as means ± SDs. $^{*}p < 0.05$.

from anaphase to telophase was 63 ± 24 min (Fig. 1B and C). In contrast, for cells overexpressing RNF213 R4810K, progression from prometaphase to metaphase was 144 ± 25 min, while the progression from anaphase to telophase was 261 ± 52 min (Fig. 1B and C). Overexpression of RNF213 R4810K resulted in several daughter cells that failed to complete cell division. For 14.8 ± 2.9% of the total cell population, cytokinesis failed to occur (Fig. 1D).

We investigated whether activation of spindle checkpoint was responsible for the delayed mitotic progression phenotype in HeLa cells overexpressing RNF213 R4810K. We inhibited spindle checkpoint by depletion of MAD2, which senses mitotic progression, and

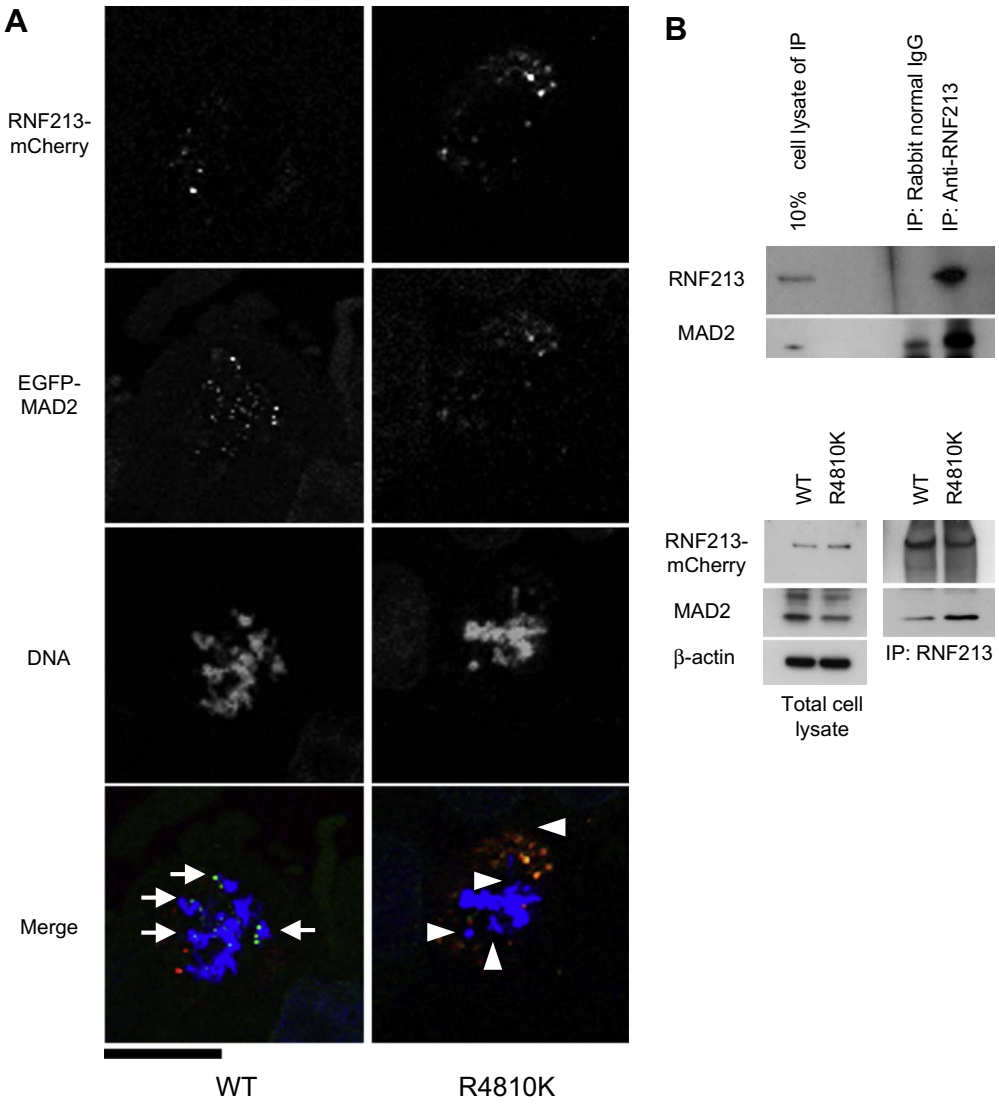

Fig. 2. Colocalization of RNF213 R4810K with MAD2 at prometaphase. (A) MAD2 localization in HeLa cells overexpressing wild-type RNF213 and RNF213 R4810K. Wild-type RNF213-mCherry (left panels; WT) or RNF213 R4810K-mCherry (right panels; R4810K) plasmids were introduced into HeLa cells stably expressing EGFP-MAD2. Red, green and blue staining corresponded to signals for RNF213-mCherry, EGFP-MAD2 and DNA, respectively. MAD2-positive lagging chromosomes in cells overexpressing wild-type RNF213 are indicated by arrows. Lagging chromosomes without MAD2 signals in cells overexpressing RNF213 R4810K are indicated by arrowheads. The scale bar indicates 20 μm. (B) Upper panel: HeLa cells were lysed and subjected to immunoprecipitation (IP) using rabbit normal IgG or an anti-RNF213 antibody. Ten-fold diluted cell lysate and the immunoprecipitated samples were immunoblotted using anti-RNF213 and anti-MAD2 antibodies. Lower panel: HeLa cells transiently expressing wild-type RNF213-mCherry (WT) or RNF213 R4810K-mCherry (R4810K) were lysed and subjected to IP using an anti-dsRed antibody. Total cell lysate and the IP samples were immunoblotted using anti-dsRed and anti-MAD2 antibodies. β-Actin was used as a loading control. (For interpretation of the references to color in this figure legend, the reader is referred to the web version of this article.)

conducted live image analysis (Fig. 1E–G). Depletion of MAD2 did not shorten the time in mitosis. In contrast, the mitotic failure rate was further increased by depletion of MAD2 in HeLa cells overexpressing RNF213 R4810K (Fig. 1H).

The localization of RNF213 was also analyzed during the mitotic phase by tracking MAD2 localization. In cells transfected with wild-type RNF213, MAD2 was localized onto the kinetochore during prometaphase, and translocated to centrosomes with RNF213 during the metaphase to anaphase transition (Figs. 2A and S4) as reported [10,11]. Signals corresponding to mCherry-tagged wild-type RNF213 were colocalized with MAD2 on mitotic microtubules around centrosomes during metaphase (Fig. S4). In contrast, we observed abnormal localization of MAD2 in cells overexpressing RNF213 R4810K. During prometaphase, MAD2 signals were not observed onto kinetochores but colocalized with RNF213 R4810K on mitotic microtubules around centrosomes (Fig. 2A). Localization of signals corresponding to mCherry-tagged RNF213 R4810K was, however, similar to that in cells overexpressing wild-type RNF213 during metaphase (Fig. S4).

The colocalization of MAD2 and RNF213 R4810K led us to investigate whether RNF213 R4810K or wild-type RNF213 could form a complex with MAD2. Both endogenous and exogenous wild-type RNF213 were co-immunoprecipitated by an anti-RNF213 antibody with endogenous MAD2 from HeLa cell extracts (Fig. 2B). A greater quantity of MAD2 was co-immunoprecipitated with the complex containing RNF213 R4810K compared with that containing wild-type RNF213. These data collectively suggest that the effects of MAD2 depletion on mitotic failure phenotype can override the mislocalization of MAD2 induced by overexpression of RNF213 R4810K in an additive manner while the effect on delayed mitotic progression phenotype is saturated.

3.2. iPSC karyotypes and mitotic abnormality in human fibroblasts

iPSCs from six fibroblast clones had normal karyotypes, but those from three MMD patients had abnormal karyotypes (Table S1, Fig. S5). The incidence of abnormal karyotypes in iPSC clones from subjects with RNF213 R4810K was 75% (3/4), while none of the six iPSC clones with wild-type RNF213 (0/6) had abnormal karyotypes (Fisher's exact test, $p < 0.03$). We then examined mitotic defects in primary fibroblasts from controls, the unaffected carrier and MMD patients (Table S1). All fibroblasts had normal karyotypes. We also searched for potential mitotic defects that may have been inherent in primary fibroblasts in patients with MMD by activating the spindle checkpoint with nocodazole. MAD2 signals and mitotic morphology were observed 72 h after treatment with nocodazole. Treatment with nocodazole depolymerizes microtubules and attached microtubules are detracted from kinetochores. Therefore, MAD2 should have been mobilized onto unattached kinetochores. In fact, in control cells, the majority of MAD2 was observed at the kinetochores. However, large quantities of MAD2 did not bind to the kinetochores of lagging chromosomes (Fig. 3) in fibroblasts from patients with RNF213 R4810K ($n = 3$, $61.0 \pm 8.2\%$) compared with those from controls ($n = 6$, $13.1 \pm 7.7\%$; $p < 0.01$). Furthermore, aneuploidy was observed more frequently in fibroblasts from MMD patients than in controls (Fig. 4A). Even under the condition of activated spindle checkpoint by nocodazole, distances of sister chromatids were widened in patient 1 and patient 2 and sister chromatids were separated completely in patient 3 (Fig. 4B). Premature sister chromatid separation can induce karyotype abnormality. Taken together these observations, the mislocalization of MAD2, aneuploidy and premature sister chromatid separation, consistently suggest mitotic abnormalities.

Next live image analyses for iPSECs from patients, Patient 1(GA), 2 (AA) and 3 (AA), an unaffected carrier (GA) and controls, Control 1 and 2 (GG) were conducted (Fig. 4C). The mean time (min) from prometaphase to metaphase was significantly longer (GA; 79.2 ± 72.1 or AA; 94.4 ± 86.3) for iPSECs from patients and unaffected carrier than from controls (42.0 ± 30.3; $p < 0.05$). However, the mean time from metaphase to anaphase for iPSECs from patients and unaffected carrier was not different from that for iPSECs from controls ($p > 0.05$). It is interesting that the mitotic failure rate (%) was also significantly higher for iPSECs from the patients and unaffected carrier (GA; 13.0 ± 3.2 or AA; 21.2 ± 4.0) than from the controls (1.9 ± 3.2; $p < 0.05$). The phenomena observed in HeLa cells overexpressing RNF213 R4810K were recaptured in iPSECs heterozygous and homozygous for RNF213 R4810K, suggesting that mitotic abnormality is genuinely associated with RNF213 R4810K.

4. Discussion

In this study, we demonstrated that RNF213 R4810K adversely affected the localization of MAD2 to the kinetochore during mitosis. Furthermore, RNF213 colocalized with MAD2 by confocal microscopy and immunoprecipitation confirmed both endogenous and exogenous wild-type RNF213 and RNF213 R4810K formed complexes with MAD2. The MAD2 complex with RNF213 R4810K captured a greater quantity of MAD2 than the complex with wild-type RNF213, suggesting a larger capturing capacity. The abnormal localization of MAD2 and mitotic abnormality were confirmed in primary fibroblasts from MMD patients. Furthermore, we observed more frequent karyotype abnormality in iPSCs from MMD patients compared with wild-type controls.

These findings indicate that RNF213 R4810K induces phenotypes associated with mitotic abnormalities. It is well known that genetic defects in cell cycle-related proteins are associated with steno-occlusive lesions around the Circle of Willis. These include Ras-MAPK pathway-related diseases (neurofibromatosis 1, Noonan syndrome, Castelo syndrome, Cranio-facio-cutaneous syndrome, and Alagille syndrome [12–14]) and cell cycle-related diseases (microcephalic osteodysplastic primordial dwarfism type II, Seckel syndrome and X-related moyamoya syndrome) [15]. The majority of cell cycle-related diseases are often accompanied by somatic undergrowth. It is likely that cell cycle defects elevate the risk of cell death or mitotic failure due to defective mitosis and chromosomal missegregation, which may be a common inherent risk factor among diseases associated with moyamoya syndrome and MMD. This would adversely affect multiple organs, including the vascular system. In contrast, MMD is not complicated by somatic undergrowth. We speculate that mitotic defects in RNF213 R4810K carriers specifically emerge in vascular endothelial cells.

The current study demonstrated an elevated mitotic failure rate in iPSECs from MMD patients. When ECs are damaged, they may be peeled off from the vascular bed and then denudated vascular areas emerge. Such vascular denudation should be recovered by migration and proliferation of circulating endothelial progenitor cells. Unless otherwise, migration and proliferation of vascular smooth muscle cells (VSMCs) occur subsequently, resulting in intimal hyperplasia. It may be considered a limitation of our work that we did not investigate VSMCs. However, given the pathological model of the vascular injury induced by radiation [16], which is known to cause steno-occlusive lesion in intracranial artery [3], an initial pathological process in MMD may be reasonably assumed to be mediated by mitotic failure of endothelial cells (ECs) followed by the excessive proliferation of VSMCs. The interactions between ECs and VSMCs play key roles in maintaining vascular structure and the function of vessels [16]. VSMC migration, proliferation, and differentiation are critical processes involved in intimal hyperplasia and are regulated by ECs [16]. Thus, mitotic failure may impair the crosstalk between ECs and VSMCs in patients with MMD. Further studies focusing on cell cycle defects in VSMCs and the crosstalk between VSMCs and endothelial cells are necessary.

In the current study, delayed mitotic progression phenotypes of HeLa cells overexpressing RNF213 R4810K or of iPSECs from patients was consistently observed. To investigate whether spindle checkpoint activation is responsible for the delayed mitotic progression phenotype, the MAD2 signaling pathway was inhibited. Depletion of MAD2 did not shorten time in mitosis or induce mitotic exit in cells overexpressing RNF213 R4810K, indicating that spindle checkpoint may be inactivated in those cells. Depletion of MAD2, however, could override the mitotic failure phenotype of HeLa cells overexpressing RNF213 R4810K in an additive manner. These observations suggest overexpression of RNF213 R4810K causes MAD2 mislocalization and leads to inactivation of MAD2 function, which is further impaired by depletion of MAD2 in the phenotype of the mitotic failure. Previously, we reported that RNF213 R4810K suppressed gene expression of *Securin*, *SKA3*, *SGO1*, *CDC20* and *BUB1*[8]. It should be noted that depletion of *SKA3* and *SGO1* cause mitotic delays and premature sister chromatid separation [17]. Taken together, for mechanisms of mitotic abnormalities, a simple and straightforward explanation would be to assume that because *Securin* has dual mechanisms of separase regulation [18] and depletion of *Securin* slowed mitotic progression [19], RNF213 R4810K slowed mitotic progression by down-regulation of *Securin* and caused mitotic abnormalities by MAD2 mislocalization [20]. However, we cannot ignore other possibilities because other down regulated genes may cause mitotic abnormalities in a synergistic manner or an antagonistic manner. The most substantial event in mitotic abnormalities, however, is likely associated with the down regulation of a group of mitosis

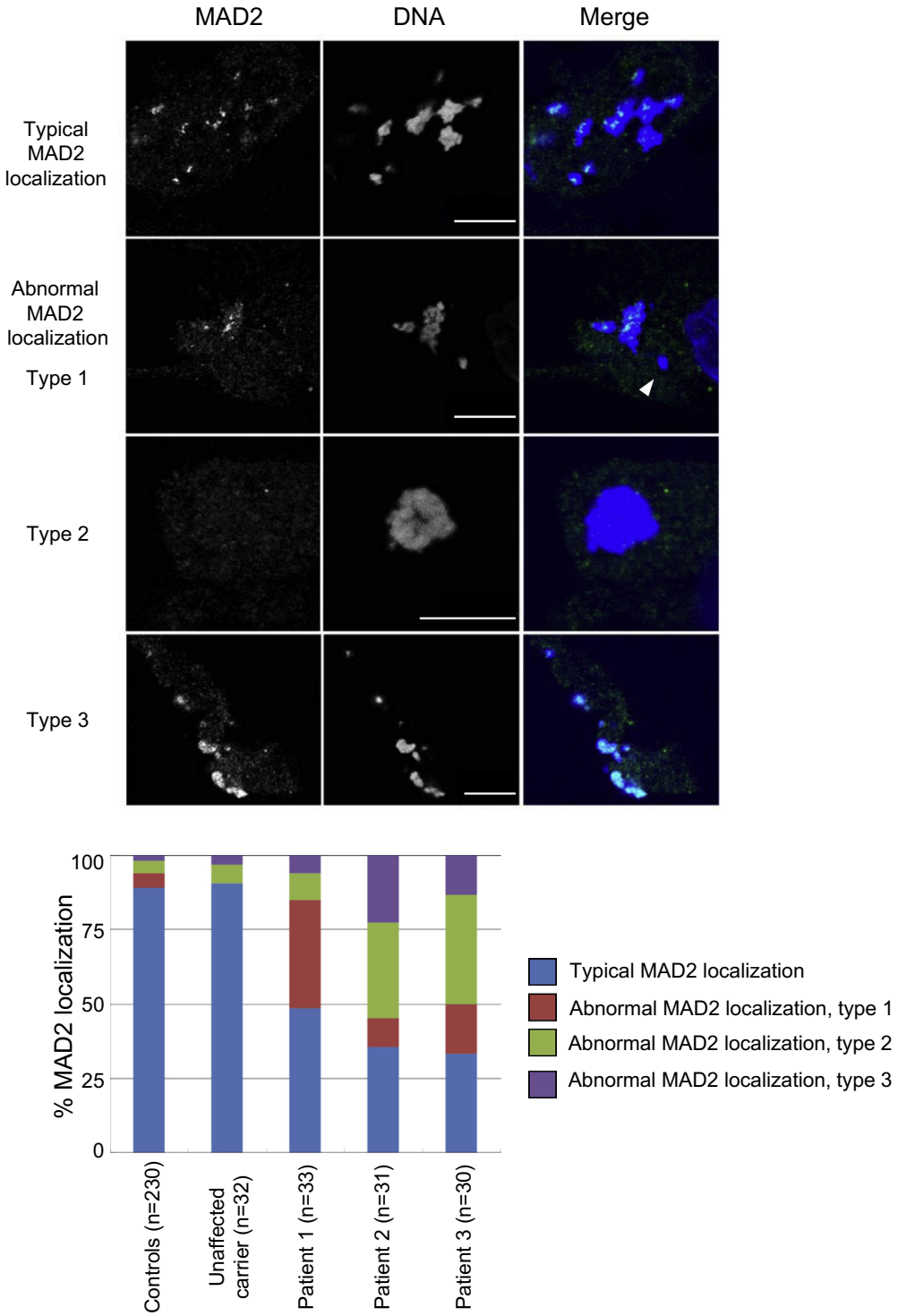

Fig. 3. Subcellular localization of MAD2 in fibroblasts from MMD patients at prometaphase. Fibroblasts from MMD patients ($n = 3$), an unaffected carrier ($n = 1$), or controls ($n = 6$) treated with nocodazole for 72 h were incubated with an antibody against MAD2. The numbers of examined chromosomes are shown in parentheses. For each subject, more than 30 chromosomes were investigated. Typical MAD2 signals (green) and nuclei (blue) in MMD fibroblasts are shown in the top panels. The scale bar represents 10 μm. Abnormal MAD2 staining patterns are shown in the lower panel. Abnormal MAD2 localization type 1 refers to MAD2-positive cells with MAD2-negative lagging chromosomes (arrowhead). Abnormal MAD2 localization type 2 refers to MAD2-negative cells. Abnormal MAD2 localization type 3 was defined as a distribution pattern of MAD2 that was not spotty, yet the protein was present and spread across the entire chromosome. The frequencies of the different MAD2 staining patterns in MMD fibroblasts were compared with controls using Fisher's exact test followed by Bonferroni correction. $p = 1.00$, unaffected carrier vs. controls; $p = 3.19 \times 10^{-11}$, patient 1 vs controls; $p = 8.77 \times 10^{-7}$, patient 2 vs controls; $p = 5.54 \times 10^{-10}$, patient 3 vs controls. (For interpretation of the references to color in this figure legend, the reader is referred to the web version of this article.)

associated genes by RNF213 R4810K. Further studies are needed to understand the mechanisms of RNF213 R4810K-induced down regulation of mitosis-associated genes and subsequent signaling deviations that induce mitotic abnormalities.

We observed an inhibition of cellular proliferation *in vitro*, but not in *ex vivo* studies [8]. We attributed these differences to acute and chronic effects. Acutely, there is very little adaptation to RNF213 R4810K overexpression; however, in chronic cases the cells

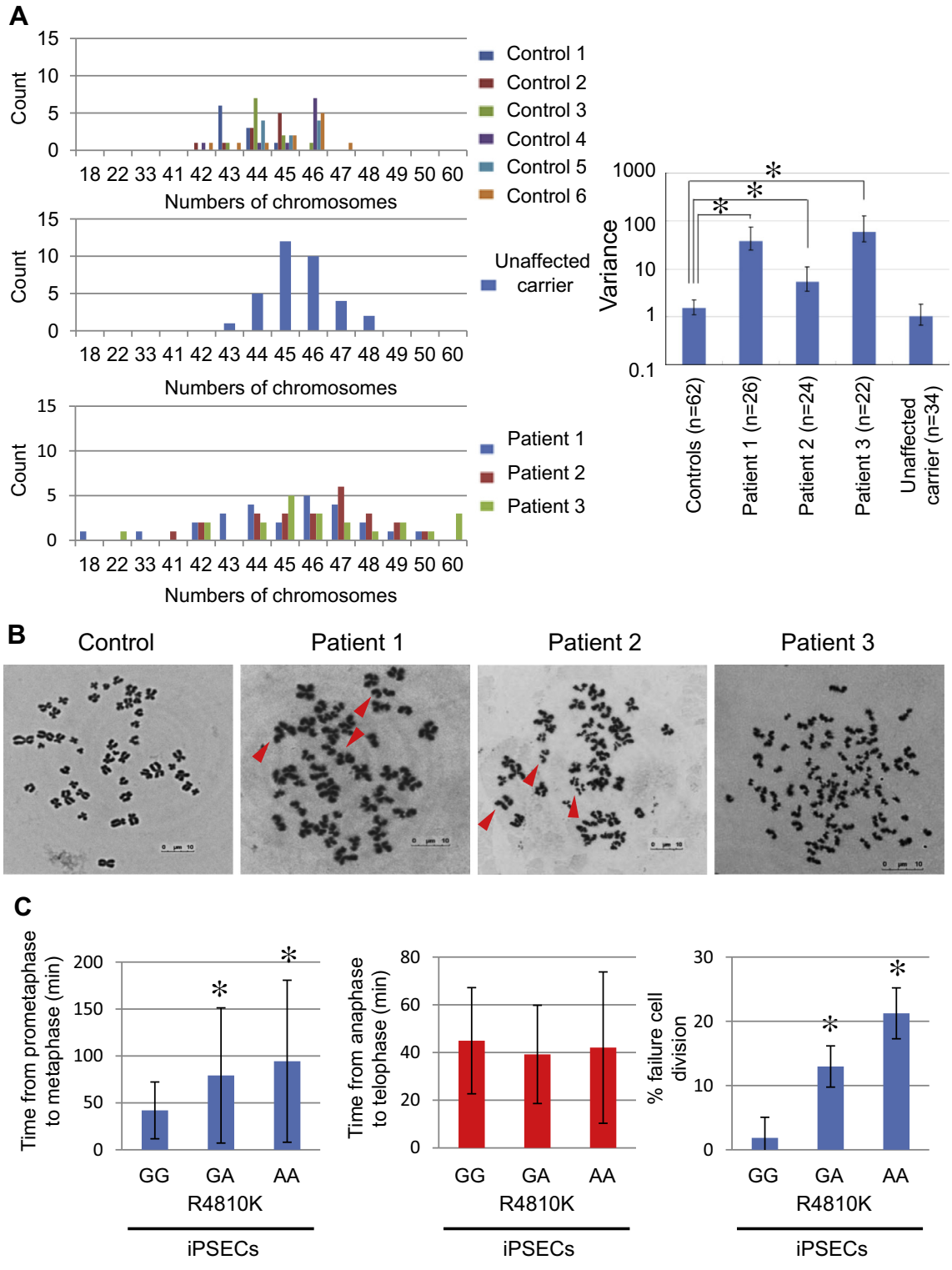

Fig. 4. Mitotic abnormality in fibroblasts and time-lapse imaging of iPSECs from MMD patients. (A) Karyotypes of MMD fibroblasts. Fibroblasts from MMD patients, the unaffected carrier or controls treated with nocodazole for 72 h were subjected to Giemsa staining. Fibroblasts from the controls (upper), carriers (middle), and MMD patients (lower) can be clearly seen. The variance in chromosome number is presented with a 95% confidence interval (right panel). Heterogeneity in the variance was tested using the *F*-test with Bonferroni correction for equality of variance. $^{*}p < 0.001$ using the *F*-test. (B) Typical morphologies of chromosomes stained with Giemsa in fibroblasts from MMD patients and controls. Prematurely separated chromosomes in the fibroblasts from patients 1 and 2 are indicated by arrowheads. Completely separated chromosomes in the fibroblasts from patient 3 are shown in the right panel. The typical morphology of fibroblasts from controls is presented in the left panel. The scale bar indicates 10 μm. (C) Time-lapse imaging of iPSECs from MMD patients and an unaffected carrier (GA or AA genotype) and controls (GG genotype). The period of time from prometaphase to metaphase, and from anaphase to telophase, and failed cell division were evaluated. Values are presented as means ± SDs. $^{*}p < 0.05$.

may adapt for the gain of function effects of this protein and mask the proliferative defects. Such discrepancies are often observed between acute and chronic effects [21–23].

In conclusion, this study demonstrated the sequestration of MAD2 by RNF213 R4810K during mitosis. The resultant defects including mitotic abnormalities were considered to increase genomic instability and thus be risk factors for MMD.

Funding sources

This work was supported by grants from the Ministry of Education, Culture, Sports, Science and Technology of Japan (Nos. 17109007 and 22249020 to Dr. Koizumi). This research was partially supported by the Japan Society for the Promotion of Science through its Funding Program for World-Leading Innovative R&D on Science and Technology (FIRST Program to Dr. Osafune).

Acknowledgments

We are grateful to Drs. Wanyang Liu, Shanika Nanayakkara, STMLD Senevirathna (Kyoto University Graduate School of Medicine) and Sasatani (Toyoshima) M (Hiroshima University) for their discussion.

Appendix A. Supplementary data

Supplementary data associated with this article can be found, in the online version, at http://dx.doi.org/10.1016/j.bbrc.2013.08.067.

References

[1] J. Suzuki, A. Takaku, Cerebrovascular "moyamoya" disease. Disease showing abnormal net-like vessels in base of brain, Arch. Neurol. 20 (1969) 288–299.
[2] K. Takeuchi, K. Shimizu, Hypogenesis of bilateral internal carotid arteries, Brain Nerv. 9 (1957) 37–43.
[3] S. Kuroda, K. Houkin, Moyamoya disease: current concepts and future perspectives, Lancet Neurol. 7 (2008) 1056–1066.
[4] W. Miao, P.L. Zhao, Y.S. Zhang, H.Y. Liu, Y. Chang, J. Ma, Q.J. Huang, Z.X. Lou, Epidemiological and clinical features of Moyamoya disease in Nanjing, China, Clin. Neurol. Neurosurg. 112 (2010) 199–203.
[5] R.M. Scott, E.R. Smith, Moyamoya disease and moyamoya syndrome, N. Engl. J. Med. 360 (2009) 1226–1237.
[6] A. Veeravagu, R. Guzman, C.G. Patil, L.C. Hou, M. Lee, G.K. Steinberg, Moyamoya disease in pediatric patients: outcomes of neurosurgical interventions, Neurosurg. Focus 24 (2008) E16.
[7] W. Liu, D. Morito, S. Takashima, Y. Mineharu, H. Kobayashi, T. Hitomi, H. Hashikata, N. Matsuura, S. Yamazaki, A. Toyoda, K. Kikuta, Y. Takagi, K.H. Harada, A. Fujiyama, R. Herzig, B. Krischek, L. Zou, J.E. Kim, M. Kitakaze, S. Miyamoto, K. Nagata, N. Hashimoto, A. Koizumi, Identification of RNF213 as a susceptibility gene for moyamoya disease and its possible role in vascular development, PLoS ONE 6 (2011) e22542.
[8] T. Hitomi, Habu, T., Kobayashi, H., Okuda, H., Harada, HK, Osafune, K., Taura, D., Sone, M., Adaka, I., Ameku, T., Watanabe, A., Kasahara, T., Sudo, T., Shiota, F., Hashikata, H., Takagi, Y., Morito, D., Miyamoto, S., Nakao K., and Koizumi, A., Down-regulation of Securin by the variant RNF213 R4810K may likely reduce angiogenic activity of induced pluripotent stem cells- derived vascular endothelial cells from moyamoya patients, Biochem. Biophys. Res. Commun. **438**, (2013), 13-19.
[9] K. Takahashi, K. Tanabe, M. Ohnuki, M. Narita, T. Ichisaka, K. Tomoda, S. Yamanaka, Induction of pluripotent stem cells from adult human fibroblasts by defined factors, Cell 131 (2007) 861–872.
[10] B.J. Howell, D.B. Hoffman, G. Fang, A.W. Murray, E.D. Salmon, Visualization of Mad2 dynamics at kinetochores, along spindle fibers, and at spindle poles in living cells, J. Cell Biol. 150 (2000) 1233–1250.
[11] Y. Li, R. Benezra, Identification of a human mitotic checkpoint gene: hsMAD2, Science 274 (1996) 246–248.
[12] W.E. Tidyman, K.A. Rauen, Noonan, Costello and cardio-facio-cutaneous syndromes: dysregulation of the Ras-MAPK pathway, Exp. Rev. Mol. Med. 10 (2008) e37.
[13] B.M. Kamath, N.B. Spinner, K.M. Emerick, A.E. Chudley, C. Booth, D.A. Piccoli, I.D. Krantz, Vascular anomalies in Alagille syndrome: a significant cause of morbidity and mortality, Circulation 109 (2004) 1354–1358.
[14] M. Noseda, L. Chang, G. McLean, J.E. Grim, B.E. Clurman, L.L. Smith, A. Karsan, Notch activation induces endothelial cell cycle arrest and participates in contact inhibition: role of p21Cip1 repression, Mol. Cell. Biol. 24 (2004) 8813–8822.
[15] A. Koizumi, H. Kobayashi, T. Hitomi, Genes associated with moyamoya syndrome and disease, No Shinkei Geka 40 (2012) 105–118.
[16] F. Milliat, A. Francois, M. Isoir, E. Deutsch, R. Tamarat, G. Tarlet, A. Atfi, P. Validire, J. Bourhis, J.C. Sabourin, M. Benderitter, Influence of endothelial cells on vascular smooth muscle cells phenotype after irradiation: implication in radiation-induced vascular damages, Am. J. Pathol. 169 (2006) 1484–1495.
[17] J.R. Daum, J.D. Wren, J.J. Daniel, S. Sivakumar, J.N. McAvoy, T.A. Potapova, G.J. Gorbsky, Ska3 is required for spindle checkpoint silencing and the maintenance of chromosome cohesion in mitosis, Curr. Biol. 19 (2009) 1467–1472.
[18] N.C. Hornig, P.P. Knowles, N.Q. McDonald, F. Uhlmann, The dual mechanism of separase regulation by securin, Curr. Biol. 12 (2002) 973–982.
[19] L.J. Holt, A.N. Krutchinsky, D.O. Morgan, Positive feedback sharpens the anaphase switch, Nature 454 (2008) 353–357.
[20] L. Michel, E. Diaz-Rodriguez, G. Narayan, E. Hernando, V.V. Murty, R. Benezra, Complete loss of the tumor suppressor MAD2 causes premature cyclin B degradation and mitotic failure in human somatic cells, Proc. Natl. Acad. Sci. USA 101 (2004) 4459–4464.
[21] F. Iovino, L. Lentini, A. Amato, A. Di Leonardo, RB acute loss induces centrosome amplification and aneuploidy in murine primary fibroblasts, Mol. Cancer 5 (2006) 38.
[22] J. Mei, X. Huang, P. Zhang, Securin is not required for cellular viability, but is required for normal growth of mouse embryonic fibroblasts, Curr. Biol. 11 (2001) 1197–1201.
[23] K. Pfleghaar, S. Heubes, J. Cox, O. Stemmann, M.R. Speicher, Securin is not required for chromosomal stability in human cells, PLoS Biol. 3 (2005) e416.